JOURNAL OF SPACECRAFT AND ROCKETS
Vol. 51, No. 1, January–February 2014

Laser Reference Sensor Alignment Estimation Using Reference Signal Observations

Noah H. Smith* and Sungkoo Bae†
University of Texas, Austin, Texas 78712
Charles E. Webb‡
Stinger Ghaffarian Technologies, Inc., Greenbelt, Maryland 20771
and
Bob E. Schutz§
University of Texas, Austin, Texas 78712

DOI: 10.2514/1.A32546

The Laser Reference Sensor is the central instrument in the Ice, Cloud, and land Elevation Satellite laser pointing knowledge system, simultaneously observing the altimetry laser, stars, and a reference signal in a single instrument coordinate frame. The reference signal is intended to provide direct observations of the alignment between the Laser Reference Sensor and the Instrument Star Tracker. The reference signal failed early in the mission and a method was developed to partially replace it by comparing two attitude time series: an attitude filter time series for the Instrument Star Tracker and a pure-gyro time series for the Laser Reference Sensor. Only the Instrument Star Tracker and gyros are used in the replacement method, with the gyros tracking the Laser Reference Sensor attitude in order to make the relative motion of the Instrument Star Tracker observable.

Nomenclature

$A_{\mathrm{LRS}}(t_k)$	=	Laser Reference Sensor attitude time series
$A_{\mathrm{IST}}(t_k)$	=	Instrument Star Tracker attitude time series
$\boldsymbol{a}(t)$	=	attitude error rotation vector with $a \equiv \lvert\boldsymbol{a}\rvert$, rad
$\hat{\boldsymbol{b}}(t)$	=	estimated gyro angular rate bias, rad/s
H	=	sensitivity matrix
h	=	measurement model
h, v	=	horizontal and vertical coordinates of a unit vector in an i, j, k frame
h_{LRSRS}	=	reference spot position in the Laser Reference Sensor frame h coordinate
h_{LRS2IST}	=	h coordinate of Laser Reference Sensor k in the Instrument Star Tracker i, j, k frame
c	=	prior estimate for h_{LRS2IST}
i, j, k	=	coordinate frame axes
K	=	Kalman gain matrix
$M(t_k)$	=	Laser Reference Sensor to Instrument Star Tracker alignment time series
P	=	state covariance matrix
Q	=	process noise covariance matrix
$q(\boldsymbol{a}(t))$	=	unit-norm attitude error quaternion function of $\boldsymbol{a}(t)$ with $q(\boldsymbol{a}(t))$
$q_{\mathrm{ref}}(t)$	=	reference attitude quaternion with $\lvert q_{\mathrm{ref}}(t)\rvert = 1$
R	=	measurement noise covariance matrix
$R(a)$	=	state transition submatrix
$S(a)$	=	state transition submatrix
$\boldsymbol{u}$	=	three-dimensional unit vector in an i, j, k frame
v_{LRSRS}	=	reference spot position in the Laser Reference Sensor frame v coordinate
v_{LRS2IST}	=	v coordinate of Laser Reference Sensor k in the Instrument Star Tracker i, j, k frame
$\bar{v}_{\mathrm{LRS2IST}}$	=	prior estimate for v_{LRS2IST}
$\boldsymbol{x}$	=	state vector
α	=	rotation from IST i to Laser Reference Sensor i about Instrument Star Tracker k, rad
$\bar{\alpha}$	=	prior estimate for α
$\Delta\alpha$	=	correction for $\bar{\alpha}$
$\Delta h_{\mathrm{LRS2IST}}$	=	correction for $\bar{h}_{\mathrm{LRS2IST}}$
$\Delta\hat{h}_{\mathrm{LRSRS}}(t_k)$	=	estimated reference spot motion time series
$\Delta v_{\mathrm{LRS2IST}}$	=	correction for $\bar{v}_{\mathrm{LRS2IST}}$
$\Delta\hat{v}_{\mathrm{LRSRS}}(t_k)$	=	estimated reference spot motion time series
ε	=	zero-mean white noise vector
$\boldsymbol{\eta}_a(t)$	=	zero-mean white noise processes associated with gyro angular random walk, rad/s
$\boldsymbol{\eta}_r(t)$	=	zero-mean white noise processes associated with gyro rate random walk, rad/s^2
θ_h, θ_v	=	angular coordinates of $\boldsymbol{u}$ in an i, j, k frame, radians
Φ	=	state transition matrix
$\hat{\boldsymbol{\omega}}(t)$	=	estimated angular rate vector, rad/s
$\boldsymbol{\omega}_g(t)$	=	gyro angular rate vector, rad/s

Received 16 November 2012; revision received 17 March 2013; accepted for publication 21 March 2013; published online 25 July 2013.

*Postdoctoral Fellow, Center for Space Research. Member AIAA.
†Research Scientist Engineer, Center for Space Research. Member AIAA.
‡Chief Scientist, Cryospheric Sciences Laboratory, Code 615, NASA Goddard Space Flight Center. Senior Member AIAA.
§Professor and Associate Director, Center for Space Research. Associate Fellow AIAA.

I. Introduction

THE Ice, Cloud, and land Elevation Satellite (ICESat) laser altimeter pointing knowledge system centers on a custom star tracker, the Laser Reference Sensor (LRS), which simultaneously observes stars and the altimetry laser in the LRS coordinate frame [1–4]. The LRS star observations are sparse due to design tradeoffs and functional limitations and it is necessary to augment them with observations from one or more conventional star trackers. The pointing knowledge system includes a custom reference signal to directly observe the alignment between the LRS and the Instrument Star Tracker (IST) [5,6]. The reference signal failed early in the mission and LRS, IST, and gyro data from before the failure were used to develop a replacement method for partially determining the relative motion between the LRS and IST [7,8]. The LRS alignment will be shown to be sufficiently stable to partially replace the reference signal using IST and gyro data.

This paper describes how reference signal observations are used to estimate alignment. It then describes how the replacement method is used to partially replace the reference signal data. We believe that

direct observation of relative alignment on-orbit using a reference signal is unusual, and that the ICESat flight data, alignment estimation method, and replacement method are of interest to the field. The flight data concerning LRS alignment stability may also be of interest.

The second section describes the hardware involved and the flight data sample. The third section describes an iterative batch least-squares method for using LRS observations of the reference spot to estimate the LRS-to-IST alignment. The fourth section describes the method developed to partially replace the reference signal. The fifth section presents results on the relative motion between the LRS and IST, and LRS alignment stability with respect to the altimetry laser.

II. Hardware Components and Flight Data Sample

The ICESat is a member of the NASA Earth Observing System. It was launched in January 2003 and deorbited in August 2010. The science instrument is the Geoscience Laser Altimeter System (GLAS), designed and constructed at NASA Goddard Space Flight Center [2,4]. The primary objective is the determination of polar ice sheet mass balances and their contribution to global sea level change. This requires highly accurate measurements of the surface elevation at each laser footprint [9–11]. The location of a footprint and its associated elevation are obtained by combining the geocentric position vector of GLAS, GLAS laser pointing, and altimeter range measurements. The accuracy requirement for surface elevation is 15 cm, which is equivalent to a laser pointing knowledge accuracy of 1.5 arcseconds.

The left side of Fig. 1 shows the LRS and IST coordinate frames. Their i, j, k axes are defined similarly and differ by a small alignment rotation $\boldsymbol{M}(t)$. The LRS and IST are mounted side-by-side on the GLAS optical bench, along with a Space Inertial Reference Unit (SIRU) gyro unit. The IST is a commercial HD-1003 star tracker with an 8×8 deg field of view and 10 Hz output, tracking up to six stars with an instrument magnitude limit of 6.2. The spacecraft telemetry includes 10 Hz samples of the 100 Hz SIRU output. The right side of Fig. 1 is a schematic of the instruments on the plane of the optical bench. The j and k axes are in the plane of the optical bench, and the i axis is upward out of the page. An optical bench coordinate frame similar to the LRS and IST coordinate frames is commonly defined, and is also commonly referred to as the GLAS coordinate frame. The intention is to minimize relative motion between the LRS and optical bench so that the LRS coordinate frame is a good proxy for the optical bench and GLAS coordinate frames.

The spacecraft is nadir pointing with an angular rate of 223 arcseconds/s about its pitch axis (orbit normal axis), with periodic pitch and roll rate deviations for calibration scans (3 deg off-nadir) and intermittent deviations for target-of-opportunity pointing (<5 deg off-nadir). During 15 of the 18 science campaigns, the pitch axis is aligned (approximately parallel or antiparallel) with the LRS and IST i axis. During the other three campaigns, the pitch axis is aligned with the j axis.

The LRS ties laser pointing observations to the celestial coordinate frame by simultaneously observing both the laser and stars in the LRS coordinate frame. The star vector observations determine the LRS attitude, or rotation between the LRS coordinate frame and the celestial coordinate frame. This concept can be implemented in a variety of ways. For example, two trackers can be joined so that their relative motion is small. Combining their output in a single data stream creates a tracker with two fields of view: one to track the laser, and one to track stars.

The implementation of the GLAS LRS is based on a single set of optics and imager. The unmodified tracker is a commercial off-the-shelf HD-1003, identical to the IST. High angular resolution is needed to achieve the required pointing knowledge accuracy. The tradeoff is a small field of view. To make more stars acquirable, the sensitivity is increased by using optics with a larger aperture. The hardware modifications are implemented in custom optics and a custom sunshade resulting in a 0.5-deg-square field of view and an instrument magnitude limit of 7.5. Three spots of light are observed and tracked: a laser spot, a reference spot, and an intermittent star spot. They are discussed in turn next.

The laser spot is generated by diverting part of the outgoing altimetry laser beam into the LRS optics. The diverted portion of the laser passes through two lateral transfer retroreflectors. The second retroreflector is shown in Fig. 1 at the entrance to the LRS optics. This provides direct observations of laser pointing in the LRS coordinate frame or, equivalently, the alignment between the LRS and the laser. The laser hardware is closely integrated with the GLAS optical bench. If the laser motion in the LRS coordinate frame is small, it is inferred that the LRS alignment is stable.

The reference spot is generated by diverting part of the altimetry laser through the Collimated Reference Source (CRS) mounted on the side of the IST, as shown in Fig. 1. The laser energy leaving the CRS is referred to as the reference signal and is redirected into the optics of the LRS by lateral transfer retroreflectors to generate the reference spot. The altimetry laser signal has two components [2]. The primary signal is a near-infrared beam with a wavelength of 1064 nm. A secondary signal for cloud and aerosol studies is generated by redirecting part of the primary signal through a frequency doubler for a green signal with a wavelength of 532 nm. The reference signal uses energy from the green component. The green signal decayed on-orbit due to problems in the laser system and the reference spot became too weak to observe, making a replacement method for observing the relative motion between the LRS and IST necessary. We believe that much of the reference spot motion represents relative motion between the LRS and IST, although there are undoubtedly systematic errors due to variations in the CRS and lateral transfer retroreflectors.

Star spots are acquired and tracked as they move quickly across the small field of view. At most, one star spot is tracked at a time and there are long gaps between stars. When the LRS was activated on-orbit, there were frequent system resets attributed to stray light bypassing or scattering from the sunshade. The resets were initially avoided by deactivating the LRS while in sunlight. A software change was made that deactivated star spot tracking in sunlight, leaving laser and reference spot tracking. The result is intermittent LRS observations of single stars while in eclipse, and none while in sunlight. The GLAS

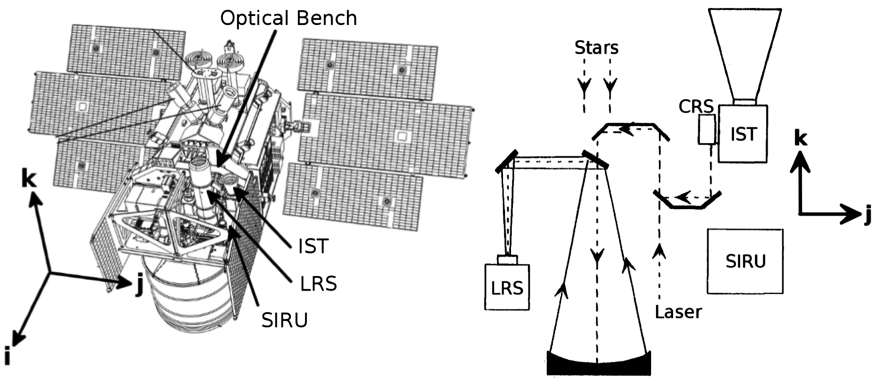

Fig. 1 LRS and IST coordinate frame axes relative to GLAS (left) and the plane of the optical bench (right).

design couples the LRS with the IST and uses the LRS star data to support observations of the LRS to IST alignment.

There is significant LRS noise associated with scattered light and with the weakening of the energy in the green laser used to generate the reference spot. Particularly when entering and leaving sunlight, scattered light degrades centroiding of the laser and references spots. Many of the resulting outliers are easily edited out, but noticeable effects remain. As the energy in the green laser decreases, the reference spot becomes dimmer and its centroid becomes more uncertain. The position variance of the output centroids grows significantly before the reference spot is lost entirely [12,13].

The results in this paper are based on a flight data sample covering 55 consecutive days in the fall of 2003, referred to as the Laser 2A (L2A) campaign. L2A is the second of 18 laser campaigns from 2003 to 2009 [2,12]. LRS reference signal observations are available for all of L2A, but become unusable soon afterwards [8,14]. The L2A observations are used to develop and test the replacement method. For consistency, the replacement method is used to produce all pointing knowledge products across the mission. The L2A observations serve as training data [7,15].

III. LRS to IST Alignment Estimation Using the Reference Signal

This section describes a method for estimating the LRS to IST alignment from observations of the reference spot and star spot. The LRS performs centroiding and geometric processing of the image pixels containing the spots and outputs three-dimensional unit vectors $\boldsymbol{u} = [\,u_1 \quad u_2 \quad u_3\,]^T$ in the LRS coordinate frame. The unit vectors can be represented as angles θ_h and θ_v from the k axis towards the i and j axes (Fig. 1). An intermediate vector $\boldsymbol{u}' = [\,h \quad v \quad 1\,]^T$ is defined, where

$$h \equiv \tan\,\theta_h = u_1/u_3 \tag{1}$$

$$v \equiv \tan\,\theta_v = u_2/u_3 \tag{2}$$

and $\boldsymbol{u}$ is the normalized version of $\boldsymbol{u}'$:

$$\boldsymbol{u} = \frac{[\,h \quad v \quad 1\,]^T}{(h^2 + v^2 + 1)^{1/2}} \tag{3}$$

Near the k axis, $h \equiv \tan\,\theta_h \cong \theta_h$ and $v \equiv \tan\,\theta_v \cong \theta_v$.

A. Alignment Representation

LRS to IST alignment is shown in Fig. 2. The i and j axes are IST coordinate frame axes. There is normally a small difference between the LRS line of sight and the IST line of sight. The LRS line of sight is a unit vector in the IST coordinate frame represented by the point h_{LRS2IST} and v_{LRS2IST}.

Besides the line-of-sight difference h_{LRS2IST} and v_{LRS2IST}, an angle α specifies the rotation of the LRS field of view. The transformation from IST coordinates to LRS coordinates is

$$\begin{bmatrix} h_{\mathrm{LRS}} \\ v_{\mathrm{LRS}} \end{bmatrix} = \begin{bmatrix} \cos\,\alpha & \sin\,\alpha \\ -\sin\,\alpha & \cos\,\alpha \end{bmatrix} \begin{bmatrix} h_{\mathrm{IST}} - h_{\mathrm{LRS2IST}} \\ v_{\mathrm{IST}} - v_{\mathrm{LRS2IST}} \end{bmatrix} \tag{4}$$

A unit vector in the IST coordinate frame

$$\boldsymbol{u}_{\mathrm{IST}} = \frac{[\,h_{\mathrm{IST}} \quad v_{\mathrm{IST}} \quad 1\,]^T}{(h_{\mathrm{IST}}^2 + v_{\mathrm{IST}}^2 + 1)^{1/2}} \tag{5}$$

is expressed in the LRS coordinate frame by

$$\boldsymbol{u}_{\mathrm{LRS}} = \frac{[\,h_{\mathrm{LRS}} \quad v_{\mathrm{LRS}} \quad 1\,]^T}{(h_{\mathrm{LRS}}^2 + v_{\mathrm{LRS}}^2 + 1)^{1/2}} \tag{6}$$

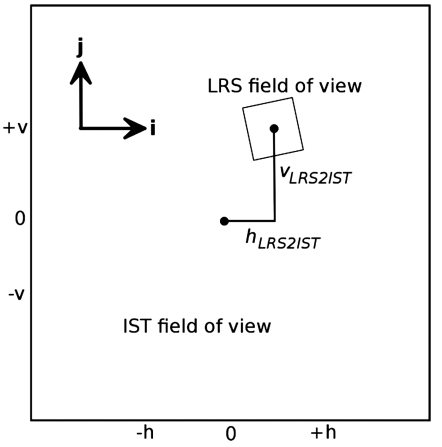

Fig. 2 LRS to IST alignment.

This conversion allows IST star observations to be used as artificial LRS star observations, or LRS laser observations to be used as artificial IST laser observations.

B. Alignment Estimation

The objective of alignment estimation using the reference signal is to determine values for the parameters h_{LRS2IST}, v_{LRS2IST}, and α. The data are LRS reference signal observations, LRS star observations, and prior parameter estimates. Batches of observations are used for least-squares parameter estimation. The batches are formed so that the parameters can be treated as constants within each batch interval. A batch can be formed using all of the observations near a specified orbit position during consecutive orbits. The orbit segment used to form a batch depends on the magnitude and rate of the parameter variations. If the parameters are constant, the batch can include observations from the entire orbit. To choose proper batch and orbit segment characteristics, the reference signal observations are used for an initial description of the parameter variations.

Equation (4) is nonlinear in the parameters to be estimated. It is linearized here about prior parameter estimates from ground calibration at launch and previous estimation results during operations. The parameters h_{LRS2IST}, v_{LRS2IST}, and α are represented as $\bar{h}_{\mathrm{LRS2IST}} + \Delta h_{\mathrm{LRS2IST}}$, $\bar{v}_{\mathrm{LRS2IST}} + \Delta v_{\mathrm{LRS2IST}}$, and $\bar{\alpha} + \Delta\alpha$, where the overbar indicates a prior parameter estimate and Δ indicates a small correction to be estimated. Substituting into Eq. (4),

$$\begin{bmatrix} h_{\mathrm{LRS}} \\ v_{\mathrm{LRS}} \end{bmatrix} = \begin{bmatrix} \cos(\bar{\alpha} + \Delta\alpha) & \sin(\bar{\alpha} + \Delta\alpha) \\ -\sin(\bar{\alpha} + \Delta\alpha) & \cos(\bar{\alpha} + \Delta\alpha) \end{bmatrix} \times \begin{bmatrix} h_{\mathrm{IST}} - (\bar{h}_{\mathrm{LRS2IST}} + \Delta h_{\mathrm{LRS2IST}}) \\ v_{\mathrm{IST}} - (\bar{v}_{\mathrm{LRS2IST}} + \Delta v_{\mathrm{LRS2IST}}) \end{bmatrix} \tag{7}$$

$$\begin{bmatrix} h_{\mathrm{LRS}} \\ v_{\mathrm{LRS}} \end{bmatrix} = \begin{bmatrix} \cos\bar{\alpha}\cos\Delta\alpha - \sin\bar{\alpha}\sin\Delta\alpha & \sin\bar{\alpha}\cos\Delta\alpha + \cos\bar{\alpha}\sin\Delta\alpha \\ -\sin\bar{\alpha}\cos\Delta\alpha - \cos\bar{\alpha}\sin\Delta\alpha & \cos\bar{\alpha}\cos\Delta\alpha - \sin\bar{\alpha}\sin\Delta\alpha \end{bmatrix} \times \begin{bmatrix} h_{\mathrm{IST}} - (\bar{h}_{\mathrm{LRS2IST}} + \Delta h_{\mathrm{LRS2IST}}) \\ v_{\mathrm{IST}} - (\bar{v}_{\mathrm{LRS2IST}} + \Delta v_{\mathrm{LRS2IST}}) \end{bmatrix} \tag{8}$$

Because the parameters and corrections are small, Eq. (8) can be written

$$\begin{bmatrix} h_{\mathrm{LRS}} \\ v_{\mathrm{LRS}} \end{bmatrix} = \begin{bmatrix} \cos\,\bar{\alpha} - (\sin\,\bar{\alpha})\Delta\alpha & \sin\,\bar{\alpha} + (\cos\,\bar{\alpha})\Delta\alpha \\ -\sin\,\bar{\alpha} - (\cos\,\bar{\alpha})\Delta\alpha & \cos\,\bar{\alpha} - (\sin\,\bar{\alpha})\Delta\alpha \end{bmatrix} \times \begin{bmatrix} h_{\mathrm{IST}} - (\bar{h}_{\mathrm{LRS2IST}} + \Delta h_{\mathrm{LRS2IST}}) \\ v_{\mathrm{IST}} - (\bar{v}_{\mathrm{LRS2IST}} + \Delta v_{\mathrm{LRS2IST}}) \end{bmatrix} \tag{9}$$

Rearranging and discarding higher-order terms yields

$$\begin{bmatrix} h_{\mathrm{LRS}} - \cos\bar{\alpha}(h_{\mathrm{IST}} - \bar{h}_{\mathrm{LRS2IST}}) - \sin\bar{\alpha}(v_{\mathrm{IST}} - \bar{v}_{\mathrm{LRS2IST}}) \\ v_{\mathrm{LRS}} + \sin\bar{\alpha}(h_{\mathrm{IST}} - \bar{h}_{\mathrm{LRS2IST}}) - \cos\bar{\alpha}(v_{\mathrm{IST}} - \bar{v}_{\mathrm{LRS2IST}}) \end{bmatrix} = \begin{bmatrix} -\cos\bar{\alpha} & -\sin\bar{\alpha} & -\sin\bar{\alpha}(h_{\mathrm{IST}} - \bar{h}_{\mathrm{IST2LRS}}) + \cos\bar{\alpha}(v_{\mathrm{IST}} - \bar{v}_{\mathrm{LRS2IST}}) \\ \sin\bar{\alpha} & -\cos\bar{\alpha} & -\cos\bar{\alpha}(h_{\mathrm{IST}} - \bar{h}_{\mathrm{IST2LRS}}) - \sin\bar{\alpha}(v_{\mathrm{IST}} - \bar{v}_{\mathrm{LRS2IST}}) \end{bmatrix} \times \begin{bmatrix} \Delta h_{\mathrm{LRS2IST}} \\ \Delta v_{\mathrm{LRS2IST}} \\ \Delta\alpha \end{bmatrix} \tag{10}$$

The LRS coordinate frame is intended to have little rotation α relative to the IST coordinate frame. Assuming this to be true,

$$\begin{bmatrix} h_{\mathrm{LRS}} - (h_{\mathrm{IST}} - \bar{h}_{\mathrm{LRS2IST}}) - \bar{\alpha}(v_{\mathrm{IST}} - \bar{v}_{\mathrm{LRS2IST}}) \\ v_{\mathrm{LRS}} - (v_{\mathrm{IST}} - \bar{v}_{\mathrm{LRS2IST}}) + \bar{\alpha}(h_{\mathrm{IST}} - \bar{h}_{\mathrm{LRS2IST}}) \end{bmatrix} = \begin{bmatrix} -1 & -\bar{\alpha} & (v_{\mathrm{IST}} - \bar{v}_{\mathrm{LRS2IST}}) - \bar{\alpha}(h_{\mathrm{IST}} - \bar{h}_{\mathrm{LRS2IST}}) \\ \bar{\alpha} & -1 & -(h_{\mathrm{IST}} - \bar{h}_{\mathrm{LRS2IST}}) - \bar{\alpha}(v_{\mathrm{IST}} - \bar{v}_{\mathrm{LRS2IST}}) \end{bmatrix} \times \begin{bmatrix} \Delta h_{\mathrm{LRS2IST}} \\ \Delta v_{\mathrm{LRS2IST}} \\ \Delta\alpha \end{bmatrix} \tag{11}$$

This is in the form $y = Hx$ with the least-squares solution $\hat{\boldsymbol{x}} = (H^T H)^{-1} H^T \boldsymbol{y}$. The observation vector $\boldsymbol{y}$ and sensitivity matrix H are built by stacking a batch of at least two independent observations, represented by h_{IST}, v_{IST}, h_{LRS}, and v_{LRS} values, and using the prior alignment estimates $\bar{h}_{\mathrm{LRS2IST}}$, $\bar{v}_{\mathrm{LRS2IST}}$, and $\bar{\alpha}$. The prior estimates are updated with the corrections $\Delta h_{\mathrm{LRS2IST}}$, $\Delta v_{\mathrm{LRS2IST}}$, and $\Delta\alpha$ and the process is iterated until the corrections become small.

The reference spot coordinates in the LRS frame are h_{LRSRS} and v_{LRSRS}. The reference signal source is rigidly attached to the IST, and the reference spot coordinates in the IST frame h_{ISTRS} and v_{ISTRS} are assumed constant. They are combined with the prior estimates $\bar{h}_{\mathrm{LRS2IST}}$ and $\bar{v}_{\mathrm{LRS2IST}}$ in a new set of variables $\bar{h} \equiv h_{\mathrm{ISTRS}} - \bar{h}_{\mathrm{LRS2IST}}$ and $\bar{v} \equiv v_{\mathrm{ISTRS}} - \bar{v}_{\mathrm{LRS2IST}}$. Substituting into Eq. (11) yields

$$\begin{bmatrix} h_{\mathrm{LRSRS}} - \bar{h} - \bar{\alpha}\,\bar{v} \\ v_{\mathrm{LRSRS}} - \bar{v} + \bar{\alpha}\,\bar{h} \end{bmatrix} = \begin{bmatrix} -1 & -\bar{\alpha} & \bar{v} - \bar{\alpha}\,\bar{h} \\ \bar{\alpha} & -1 & -\bar{h} - \bar{\alpha}\,\bar{v} \end{bmatrix} \begin{bmatrix} \Delta h_{\mathrm{LRS2IST}} \\ \Delta v_{\mathrm{LRS2IST}} \\ \Delta\alpha \end{bmatrix} \tag{12}$$

In Eq. (12), the alignment corrections $\Delta h_{\mathrm{IST2LRS}}$, $\Delta v_{\mathrm{IST2LRS}}$, and $\Delta\alpha$ depend on the LRS observations of the reference spot h_{LRSRS} and v_{LRSRS} and on the prior knowledge of $\bar{h}$, $\bar{v}$, and $\bar{\alpha}$. The corrections are estimated based on motion of the LRS reference spot and become zero when the reference spot position is constant.

The prior alignment estimate can come from pre-launch calibration or previous alignment estimates. New estimates can be made using simultaneous LRS and IST observations of a star. Simultaneous star observations are intermittent and sparse but can be batched to generate an adequate alignment estimate for bootstrapping the algorithm into operation. Given a prior alignment estimate, a correction is estimated using a batch of LRS reference spot observations. Further batches of LRS observations from adjacent orbit positions can be used to advance the estimate in time.

IV. Method to Partially Replace the Reference Signal

The replacement method estimates the relative motion of the reference spot

$$\Delta\hat{h}_{\mathrm{LRSRS}}(t_k) \equiv \hat{h}_{\mathrm{LRSRS}}(t_k) - \hat{h}_{\mathrm{LRSRS}}(t_0) \tag{13}$$

$$\Delta\hat{v}_{\mathrm{LRSRS}}(t_k) \equiv \hat{v}_{\mathrm{LRSRS}}(t_k) - \hat{v}_{\mathrm{LRSRS}}(t_0) \tag{14}$$

by comparing attitude time series for the LRS and IST. The IST attitude time series $\hat{\boldsymbol{A}}_{\mathrm{IST}}(t_k)$ is estimated using a standard attitude filter. For the LRS attitude time series $\hat{\boldsymbol{A}}_{\mathrm{LRS}}(t_k)$, an initial estimate is propagated forward over an orbit using gyros alone. Because the alignment of the LRS and gyro unit is sufficiently stable, gyro propagation provides adequate tracking of the LRS attitude to make the relative motion of the IST partially observable. The true LRS to IST alignment time series is defined as

$$\boldsymbol{M}(t_k) \equiv \boldsymbol{A}_{\mathrm{LRS}}(t_k)\boldsymbol{A}^T_{\mathrm{IST}}(t_k) \tag{15}$$

where $\boldsymbol{A}_{\mathrm{LRS}}(t_k)$ and $\boldsymbol{A}_{\mathrm{IST}}(t_k)$ are the true attitudes. The results section demonstrates that the estimate

$$\hat{\boldsymbol{M}}(t_k) \equiv \hat{\boldsymbol{A}}_{\mathrm{LRS}}(t_k)\hat{\boldsymbol{A}}^T_{\mathrm{IST}}(t_k) \tag{16}$$

matches important features of $\boldsymbol{M}(t_k)$.

The focus of the replacement method is on observing the variations of $\hat{\boldsymbol{M}}(t_k)$. The results are less sensitive to the initial condition than they are to the time series $\boldsymbol{\omega}_g(t_k)$ and $\hat{\boldsymbol{b}}(t_k)$ used to propagate $\boldsymbol{A}_{\mathrm{LRS}}(t_k)$. The LRS and IST attitudes are similar: $\boldsymbol{A}_{\mathrm{LRS}}(t_0) \cong \boldsymbol{A}_{\mathrm{IST}}(t_0)$ and $\boldsymbol{M}(t_k)$ is a small rotation. Different initial conditions $\hat{\boldsymbol{A}}_{\mathrm{LRS},1}(t_0) = \boldsymbol{A}_{\mathrm{LRS}}(t_0)$ and $\hat{\boldsymbol{A}}_{\mathrm{LRS},2}(t_0) = \hat{\boldsymbol{A}}_{\mathrm{IST}}(t_0)$ result in time series $\hat{\boldsymbol{M}}_1(t_k)$ and $\hat{\boldsymbol{M}}_2(t_k)$ for which

$$\mathrm{d}\hat{\boldsymbol{M}}_1(t_k)/\mathrm{d}t \cong \mathrm{d}\hat{\boldsymbol{M}}_2(t_k)/\mathrm{d}t \tag{17}$$

and the results from the replacement method are approximately the same. In practice, the initial condition $\hat{\boldsymbol{A}}_{\mathrm{LRS}}(t_0) = \hat{\boldsymbol{A}}_{\mathrm{IST}}(t_0)$ is used because $\hat{\boldsymbol{A}}_{\mathrm{IST}}(t_0)$ is relatively well known from IST star observations.

The alignments $\hat{\boldsymbol{M}}(t_k)$ are computed at each point in the time series using Eq. (16) and converted to a time series of rotation vectors:

$$\hat{\boldsymbol{a}}(\hat{\boldsymbol{M}}(t_k)) \equiv [\,\hat{a}_1(t_k) \quad \hat{a}_2(t_k) \quad \hat{a}_3(t_k)\,]^T \tag{18}$$

The angles $\hat{a}_1(t_k) - \hat{a}_1(t_0)$ and $\hat{a}_2(t_k) - \hat{a}_2(t_0)$ are approximately equivalent to $\Delta\hat{h}_{\mathrm{LRSRS}}(t_k)$ and $\Delta\hat{v}_{\mathrm{LRSRS}}(t_k)$. Rotation about the i axis is approximately a change of v_{LRSRS} position and rotation about the j axis is approximately a change of h_{LRSRS} position:

$$\Delta\hat{h}_{\mathrm{LRSRS}}(t_k) \equiv \hat{h}_{\mathrm{LRSRS}}(t_k) - \hat{h}_{\mathrm{LRSRS}}(t_0) \cong \hat{a}_2(t_k) - \hat{a}_2(t_0) \tag{19}$$

$$\Delta\hat{v}_{\mathrm{LRSRS}}(t_k) \equiv \hat{v}_{\mathrm{LRSRS}}(t_k) - \hat{v}_{\mathrm{LRSRS}}(t_0) \cong \hat{a}_1(t_k) - \hat{a}_1(t_0) \tag{20}$$

These expressions convert $\hat{\boldsymbol{a}}[\hat{\boldsymbol{M}}(t_k)]$ to a partial replacement for the LRS reference signal observations in Eq. (12). They also link the reference signal observations during the L2A campaign with the replacement method results. In the results section, both the reference signal observations and the replacement method results are expressed as $\Delta\hat{h}_{\mathrm{LRSRS}}(t_k)$ and $\Delta\hat{v}_{\mathrm{LRSRS}}(t_k)$.

This section discusses estimation of $\hat{\boldsymbol{A}}_{\mathrm{IST}}(t_k)$ from orbit midnight at t_0 to the next orbit midnight at $t_0 + 5790$ s using an attitude filter combining IST and gyro data. It then discusses estimation of $\hat{\boldsymbol{A}}_{\mathrm{LRS}}(t_k)$ for the same time interval using $\boldsymbol{\omega}_g(t_k)$ and $\hat{\boldsymbol{b}}(t_k)$. In all cases, the t_k are the times of the 10 Hz IST measurements and corresponding attitude filter measurement updates. The asynchronous gyro rates $\boldsymbol{\omega}_g(t_k)$ and LRS reference signal measurements are interpolated to the IST measurement times.

A. IST Attitude Time Series

$\hat{\boldsymbol{A}}_{\mathrm{IST}}(t_k)$ is estimated using a standard attitude filter, referred to in [16] as the Multiplicative Extended Kalman Filter (MEKF). The description here follows [16,17]. The filter performs unconstrained estimation of the attitude error rotation vector $\boldsymbol{a}(t)$ during each measurement update phase while maintaining the overall attitude estimate in the unit-norm reference attitude quaternion $q_{\mathrm{ref}}(t)$. The true attitude $q(t)$ is given by $q(t) = q(\boldsymbol{a}(t)) \otimes q_{\mathrm{ref}}(t)$ where $q(\boldsymbol{a}(t))$

is a unit-norm quaternion function of the rotation vector. The measurement update phase assigns a finite value $\hat{\boldsymbol{a}}(+)$ to $\hat{\boldsymbol{a}}(t)$ while the reference quaternion retains its pre-update value $q_{\text{ref}}(-)$. The update information is moved from $\hat{\boldsymbol{a}}(+)$ to a post-update reference $q_{\text{ref}}(+)$ and $\hat{\boldsymbol{a}}(t)$ is reset to zero so that $q(\hat{\boldsymbol{a}}(+)) \otimes q_{\text{ref}}(-) = q(\boldsymbol{0}) \otimes q_{\text{ref}}(+)$.

The gyro unit outputs time-tagged angular increments that are used to compute the rate vector $\boldsymbol{\omega}_g(t)$. The true rate $\boldsymbol{\omega}(t)$ is modeled by $\boldsymbol{\omega}(t) = \boldsymbol{\omega}_g(t) + \boldsymbol{b}(t) + \boldsymbol{\eta}_a(t)$ where $\mathrm{d}\boldsymbol{b}(t)/\mathrm{d}t = \boldsymbol{\eta}_r(t)$. The angular rate estimate is $\hat{\boldsymbol{\omega}}(t_k) = \boldsymbol{\omega}_g(t_k) + \hat{\boldsymbol{b}}(t_k)$ and the propagation rotation vector is given by $\boldsymbol{a}_p = \Delta t \hat{\boldsymbol{\omega}}(t_k)$ where the time interval $\Delta t \equiv t_{k+1} - t_k$ is short enough that $\hat{\boldsymbol{\omega}}$ is approximately constant. Attitude propagation when the assumption of approximately constant $\hat{\boldsymbol{\omega}}$ is not valid is discussed in [18]. Attitude and state propagations are given by $q_{\text{ref}}(t_{k+1}) = q(\boldsymbol{a}_p) \otimes q_{\text{ref}}(t_k)$ and $\hat{\boldsymbol{x}}(t_{k+1}) = \hat{\boldsymbol{x}}(t_k)$. Covariance propagation is given by $\boldsymbol{P}_{k+1} = \boldsymbol{\Phi}_k \boldsymbol{P}_k \boldsymbol{\Phi}_k^T + \boldsymbol{Q}_k$. The state transition definitions in Eqs. (21–23) are also used next in batch least-squares differential correction for gyro bias estimation:

$$\Phi_k = \begin{bmatrix} \boldsymbol{R}(\boldsymbol{a}_p) & \boldsymbol{S}(\boldsymbol{a}_p) \\ 0 & \boldsymbol{I} \end{bmatrix} \tag{21}$$

$$\boldsymbol{R}(\boldsymbol{a}) = (\cos a)\boldsymbol{I} - \left(\frac{\sin a}{a}\right)[\boldsymbol{a}\times] + \left(\frac{1-\cos a}{a^2}\right)\boldsymbol{a}\boldsymbol{a}^T \tag{22}$$

$$\boldsymbol{S}(\boldsymbol{a}) = \Delta t\left[\left(\frac{\sin a}{a}\right)\boldsymbol{I} - \left(\frac{1-\cos a}{a^2}\right)[\boldsymbol{a}\times] + \left(\frac{a-\sin a}{a^3}\right)\boldsymbol{a}\boldsymbol{a}^T\right] \tag{23}$$

The measurement model is

$$\boldsymbol{y} \equiv \boldsymbol{h}(\boldsymbol{u}) + \boldsymbol{\varepsilon} = \begin{bmatrix} u_1/u_3 \\ u_2/u_3 \end{bmatrix} + \boldsymbol{\varepsilon} \tag{24}$$

where $\boldsymbol{\varepsilon}$ is zero-mean white noise and the measurement covariance is $\boldsymbol{R} = \sigma_y^2 \boldsymbol{I}$. For an observed unit vector $\boldsymbol{u}$ with a corresponding reference unit vector $\boldsymbol{u}'$ in the inertial frame, the observation residual is $\Delta\boldsymbol{y} \equiv \boldsymbol{y} - \boldsymbol{h}(\boldsymbol{A}(q_{\text{ref}})\boldsymbol{u}')$ and, with $[\boldsymbol{a}\times]\boldsymbol{b} \equiv \boldsymbol{a} \times \boldsymbol{b}$, the sensitivity matrix is given by

$$H = \begin{bmatrix} 1/u_3 & 0 & -u_1/u_3^2 \\ 0 & 1/u_3 & -u_2/u_3^2 \end{bmatrix}[\boldsymbol{A}(q_{\text{ref}})\boldsymbol{u}'\times] \tag{25}$$

After propagation of the state and covariance from t_k to t_{k+1}, the measurement update at t_{k+1} is performed using the Kalman gain $\boldsymbol{K} = \boldsymbol{P}\boldsymbol{H}^T(\boldsymbol{H}\boldsymbol{P}\boldsymbol{H}^T + \boldsymbol{R})^{-1}$, state correction $[\,\Delta\hat{\boldsymbol{a}}^T(t) \quad \Delta\hat{\boldsymbol{b}}^T(t)\,]^T = \boldsymbol{K}\Delta\boldsymbol{y}$, and covariance update $\boldsymbol{P}_+ = (\boldsymbol{I} - \boldsymbol{K}\boldsymbol{H})\boldsymbol{P}_-$. The rate bias estimate is updated by $\hat{\boldsymbol{b}}_+ = \hat{\boldsymbol{b}}_- + \Delta\hat{\boldsymbol{b}}$ and the attitude error estimate is moved into the reference attitude $q_{\text{ref}+} = q(\Delta\hat{\boldsymbol{a}}) \otimes q_{\text{ref}-}$. The IST attitude time series $\hat{\boldsymbol{A}}_{\text{IST}}(t_k)$ is expressed as quaternions $q_{\text{ref}}(t_k)$ or as equivalent rotation matrices as convenient. MEKF filtering of 10 Hz IST star observations with 10 Hz gyro angular rates results in arcsecond level accuracies [19].

B. LRS Attitude Time Series

Gyro propagation from the initial condition $\hat{\boldsymbol{A}}_{\text{LRS}}(t_0) = \hat{\boldsymbol{A}}_{\text{IST}}(t_0)$ is used to estimate $\hat{\boldsymbol{A}}_{\text{LRS}}(t_k)$ using time series of gyro rates $\boldsymbol{\omega}_g(t_k)$ and rate bias estimates $\hat{\boldsymbol{b}}(t_k)$. What is needed is an adequate $\hat{\boldsymbol{b}}(t_k)$ and it is estimated here using batch least-squares differential correction. The batch processor estimates an initial gyro rate bias $\hat{\boldsymbol{b}}(t_0)$ for the batch interval and $\hat{\boldsymbol{b}}(t_k)$ is then assumed constant $\hat{\boldsymbol{b}}(t_k) \equiv \hat{\boldsymbol{b}}(t_0)$. The batch consists of IST star observations $\boldsymbol{y}_i$; $i = 1, \ldots, n$ and gyro rates $\boldsymbol{\omega}_g(t_k)$, along with prior estimates of $\hat{\boldsymbol{A}}_{\text{IST}}(t_0)$ and $\hat{\boldsymbol{b}}(t_0)$. An alternative for estimating $\hat{\boldsymbol{b}}(t_0)$ is to use a $\hat{\boldsymbol{b}}$ value from an attitude filter that has processed enough IST measurement updates to converge.

This description of batch least-squares differential correction for attitude and gyro bias estimation follows [20]. The batch is processed iteratively. In each iteration, an attitude correction $\Delta\hat{\boldsymbol{a}}$ and rate bias correction $\Delta\hat{\boldsymbol{b}}$ are estimated and applied to $\hat{\boldsymbol{A}}_{\text{IST}}(t_0)$ and $\hat{\boldsymbol{b}}(t_0)$ for use in the next iteration. When $\Delta\hat{\boldsymbol{a}}$ and $\Delta\hat{\boldsymbol{b}}$ become small, the iterations are stopped.

In each iteration, a time series of attitude estimates $\hat{\boldsymbol{A}}_{\text{IST}}(t_i)$ is computed by propagating $\hat{\boldsymbol{A}}_{\text{IST}}(t_0)$ forward in time using $\boldsymbol{\omega}_g(t)$ and $\hat{\boldsymbol{b}}(t_0)$. The estimated angular rate is $\hat{\boldsymbol{\omega}}(t_i) = \boldsymbol{\omega}_g(t_i) + \hat{\boldsymbol{b}}(t_0)$ and the propagation rotation vector is given by $\boldsymbol{a}_p = \Delta t\hat{\boldsymbol{\omega}}(t_i)$, where the time interval is short enough that $\hat{\boldsymbol{\omega}}$ is approximately constant. Propagation is performed using

$$\hat{\boldsymbol{A}}(t_{i+1}) = \boldsymbol{R}(t_{i+1}, t_0)\hat{\boldsymbol{A}}(t_0) \tag{26}$$

where the state transition submatrix $\boldsymbol{R}(t_{i+1}, t_0)$ is computed recursively beginning with $\boldsymbol{R}(t_0, t_0) = \boldsymbol{I}_{3\times3}$,

$$\boldsymbol{R}(t_{i+1}, t_0) = \boldsymbol{R}(t_{i+1}, t_i)\boldsymbol{R}(t_i, t_0) = \boldsymbol{R}(\boldsymbol{a}_p)\boldsymbol{R}(t_i, t_0) \tag{27}$$

and $\boldsymbol{R}(\boldsymbol{a})$ is defined in Eq. (22). The $\boldsymbol{R}$ matrices must be orthonormal rotation matrices. This can be ensured by converting to a quaternion, normalizing, and converting back to a rotation matrix. The state transition submatrix $\boldsymbol{S}(t_{i+1}, t_0)$ is also computed recursively beginning with $\boldsymbol{S}(t_0, t_0) = \boldsymbol{0}_{3\times3}$,

$$\begin{aligned} \boldsymbol{S}(t_{i+1}, t_0) &= \boldsymbol{S}(t_{i+1}, t_i) + \boldsymbol{R}(t_{i+1}, t_i)\boldsymbol{S}(t_i, t_0) \\ &= \boldsymbol{S}(\boldsymbol{a}_p) + \boldsymbol{R}(\boldsymbol{a}_p)\boldsymbol{S}(t_i, t_0) \end{aligned} \tag{28}$$

where $\boldsymbol{S}(\boldsymbol{a})$ is defined in Eq. (23).

The gyro propagated attitudes $\hat{\boldsymbol{A}}(t_i)$ are used to compute predictions of the star observations. For a star observation $\boldsymbol{y}_i$ with an observed vector $\boldsymbol{u}$ in the tracker coordinate frame and a catalog vector $\boldsymbol{u}'$ in the celestial coordinate frame, the predicted vector in the tracker coordinate frame is $\boldsymbol{u}'' = \hat{\boldsymbol{A}}(t_i)\boldsymbol{u}'$. The measurement noise variance for $\boldsymbol{y}_i$ is σ_i^2 and the effective observation is the residual $\Delta\boldsymbol{y}_i = \boldsymbol{y}_i - \boldsymbol{h}(\boldsymbol{u}''_i)$, using the measurement model from Eq. (24).

The correction vector is $\Delta\hat{\boldsymbol{x}} \equiv [\Delta\,\hat{\boldsymbol{a}}^T \quad \Delta\hat{\boldsymbol{b}}^T\,]^T$ and the observation residual is $\Delta\boldsymbol{y}_i \equiv \boldsymbol{H}_i\Delta\hat{\boldsymbol{x}} + \boldsymbol{\varepsilon}_i$ where the measurement sensitivity is

$$\boldsymbol{H}_i = \begin{bmatrix} 1/u_3 & 0 & -u_1/u_3^2 \\ 0 & 1/u_3 & -u_2/u_3^2 \end{bmatrix}[\boldsymbol{u}_i\times][\,\boldsymbol{R}(t_i, t_0) \quad \boldsymbol{S}(t_i, t_0)\,] \tag{29}$$

The least-squares solution minimizing the sum of the squares of $\boldsymbol{\varepsilon}_i$ is

$$\Delta\hat{\boldsymbol{x}} = \left(\sum_{i=1}^{n} \sigma_i^{-2}\boldsymbol{H}_i^T\boldsymbol{H}_i\right)^{-1} \sum_{i=1}^{n} \sigma_i^{-2}\boldsymbol{H}_i^T\Delta\boldsymbol{y}_i \tag{30}$$

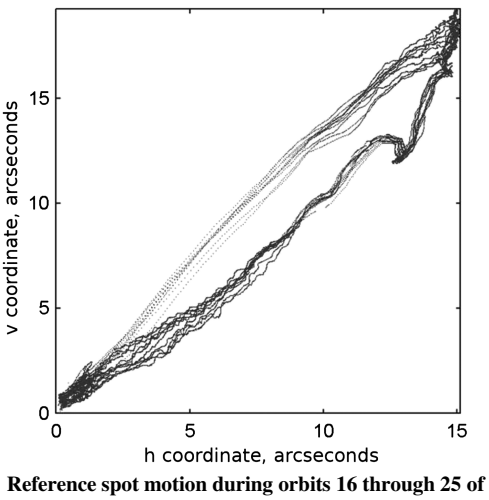

Fig. 3 Reference spot motion during orbits 16 through 25 of L2A.

To end each iteration, the corrections are applied using $\hat{\boldsymbol{b}}(t_0)_+ = \hat{\boldsymbol{b}}(t_0)_- + \Delta\hat{\boldsymbol{b}}$ and $\hat{\boldsymbol{A}}(t_0)_+ = \boldsymbol{R}(\Delta\hat{\boldsymbol{a}})\hat{\boldsymbol{A}}(t_0)_-$.

Because all of the observations in batch differential correction are transitioned backwards in time to t_0, time as a variable and information about variations with respect to time are deemphasized. The useful result here is a single point $\hat{\boldsymbol{b}}(t_0)$ representing a cluster of observations at t_0 and it is natural to interpret this point as a type of expected or mean value for the batch, given the observations.

V. LRS Alignment Results

Figure 3 shows the motion of the reference signal during orbits 16 through 25 of the L2A campaign. These orbits are from the first full day of the campaign (26 September 2003). The magnitude, shape, and other characteristics of the motion are representative for L2A as a whole. The motion evolved over the campaign, but maintained anamplitude of approximately 15 to 20 arcseconds.

Time series of the horizontal and vertical components of the motion during orbits 16 through 25 are shown in Fig. 4. The amplitude of the vertical motion varies slightly over these 10 orbits, with a decrease in amplitude in the first six orbits followed by an increase in the last four orbits. These changes are apparent in Fig. 3 as variations of the path traced by the reference signal. In the upper right corner, the reference signal path changes from orbit to orbit.

Orbits 16 through 25 are early in the L2A campaign when the green laser energy and reference signal are strong and the noise is small. The data plotted in the figures are smoothed with a moving average filter to further reduce the effects of outliers due to scattered light when entering and leaving sunlight. These events are apparent in Fig. 4 as a notch or discontinuity at the beginning of each peak. The peaks correspond to the sunlit portion of each orbit and the discontinuity occurs when entering sunlight.

Time series of the peak-to-peak amplitudes of the reference signal motion are shown in Fig. 5. The time series consist of amplitudes for each of the 821 orbits during L2A. The means and standard deviations are 14.4 ± 0.8 arcseconds for the horizontal amplitudes and 17.1 ± 2.0 arcseconds for the vertical amplitudes.

There are two commanded temperature events during L2A, as shown in Fig. 6. Both of these events are associated with GLAS reconfiguration commands from the ground. Their effects are apparent in Fig. 5 near orbit 300 and orbit 500. Twelve outliers during the events are edited out of the time series. The measurements in Fig. 6 are from a temperature sensor associated with the LRS and indicate the magnitude of the temperature events. In Fig. 5, there are changes near orbits 650 and 750 that may be associated with temperature, but we are not aware of temperature data that confirms this. The variations near orbits 200, 650, and 750 may reflect changes of the scattered light conditions. The noise and outliers caused by scattered light can affect the amplitude estimates.

The replacement method is demonstrated here for orbit 235. This is an orbit from a day (11 October 2003) that was studied intensively during the development and testing of the replacement method. Raw LRS observations of the reference signal are shown in Fig. 7. There is one time interval with a scattered light problem as the spacecraft entered sunlight. The block of points near 2000 s is a dense cluster of outliers with many values extending beyond the range of the vertical scale. Outside of this interval, the reference spot is measured to

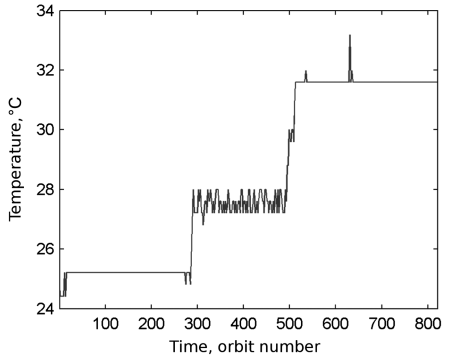

Fig. 6 Temperature measurements from a sensor associated with the LRS during L2A.

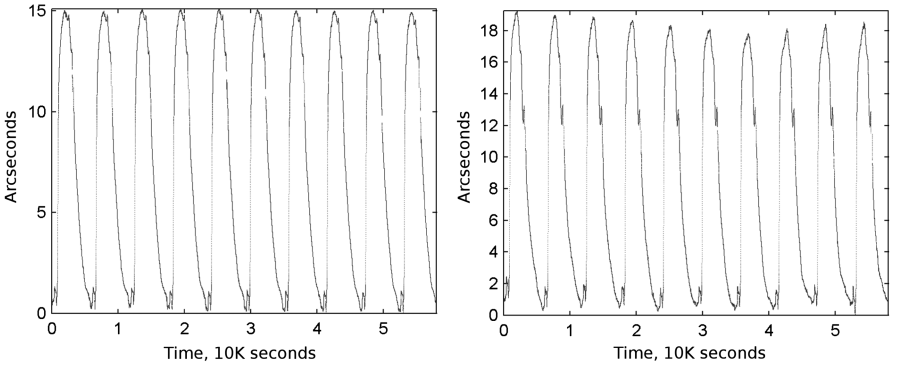

Fig. 4 Reference spot horizontal (left) and vertical (right) motion during orbits 16 through 25 of L2A.

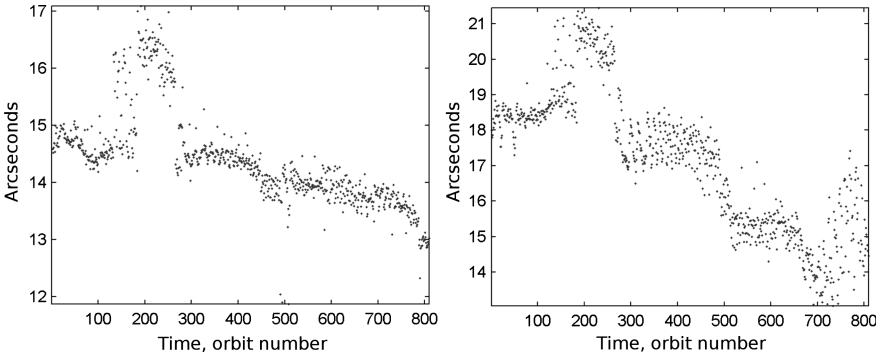

Fig. 5 Reference spot motion horizontal (left) and vertical (right) amplitudes during L2A.

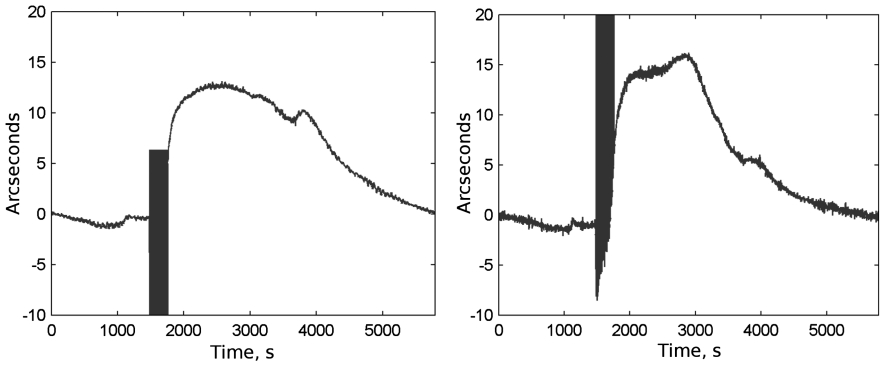

Fig. 7 Raw reference signal horizontal (left) and vertical (right) motion during orbit 235.

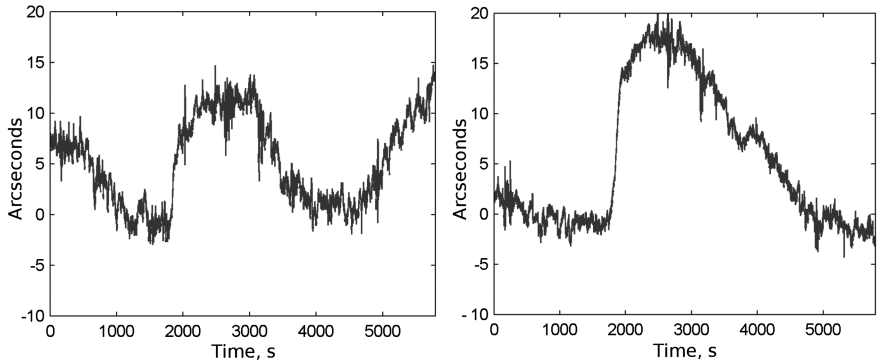

Fig. 8 Replacement method estimated reference signal horizontal (left) and vertical (right) motion for orbit 235.

an accuracy of approximately one arcsecond. Periods of slightly increased measurement noise are apparent, particularly in the vertical motion.

The replacement method results $\Delta\hat{h}_{\mathrm{LRSRS}}(t_k)$ and $\Delta\hat{v}_{\mathrm{LRSRS}}(t_k)$ for orbit 235 are shown in Fig. 8. The replacement method is a partial replacement for the reference signal and has significant limitations in practice. This is particularly true in the sense that little automation is possible. It depends on interactive decision making and interpretation. Each of the 18 laser campaigns is handled individually, with tens of hours required per campaign for experimentation and evolution of a campaign-wide result. The time series extend from orbit midnight to orbit midnight and the jump or step-change near 2000 s corresponds to entering sunlight. The time and magnitude of the jump can be estimated from these results.

We observe a general characteristic of the replacement method results. For the 15 campaigns in which the spacecraft pitch axis is aligned (approximately parallel or antiparallel) with the LRS and IST i axes, the $\Delta\hat{v}_{\mathrm{LRSRS}}(t_k)$ results are better than the $\Delta\hat{h}_{\mathrm{LRSRS}}(t_k)$ results. This is demonstrated by Fig. 8. During orbit 235, the pitch axis is aligned with the i axes and the match between $\Delta\hat{v}_{\mathrm{LRSRS}}(t_k)$ in Fig. 8 and $\Delta v_{\mathrm{LRSRS}}(t_k)$ in Fig. 7 is better than the match between $\Delta\hat{h}_{\mathrm{LRSRS}}(t_k)$ and $\Delta h_{\mathrm{LRSRS}}(t_k)$.

Two possible causes for the difference between the $\Delta\hat{h}_{\mathrm{LRSRS}}(t_k)$ and $\Delta\hat{v}_{\mathrm{LRSRS}}(t_k)$ results are the IST star measurements and the gyro angular rates $\boldsymbol{\omega}_g(t_k)$. Because the pitch axis is aligned with the IST i axis, the v coordinates of stars change at a rate of 223 arcseconds/s and the h coordinates are approximately constant. Expressing $\boldsymbol{\omega}_g(t_k)$ in the IST coordinate frame, the rate about the i axis is 223 arcseconds/s and the rate about the j axis is approximately zero.

Two types of analyses are used to evaluate the effects of the replacement method over all 18 laser campaigns. The first involves using the ocean surface as a reference and performing periodic calibration maneuvers. This is referred to as ocean scan calibration [10,11,21]. Ocean scans confirm that the replacement method significantly reduces biases in the laser pointing estimates.

The second type of analysis uses points where the laser ground tracks cross and multiple surface elevation results are available for comparison. This is referred to as crossover analysis [9]. The elevation results from multiple passes over a point on Earth's surface are used to compute mean elevation differences and elevation variances. Overall crossover statistics are then computed for Antarctica and Greenland. The elevation variances represent a measure of the uncertainty in the elevation results. Table 1 shows the elevation

Table 1 Standard deviations of surface elevations for Antarctica and Greenland crossovers

	Antarctica		Greenland	
Campaign	Uncorrected, cm	Corrected, cm	Uncorrected, cm	Corrected, cm
L1A 2003	27	21	30	23
L3B 2005	24	20	35	33
L3C 2005	24	14	62	32
L3E 2006	16	12	23	13

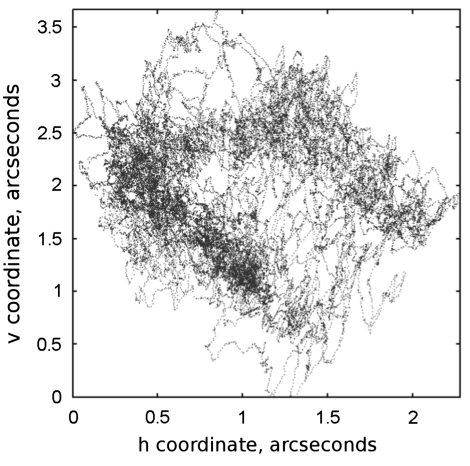

Fig. 9 Laser spot motion during orbits 16 through 25 of L2A.

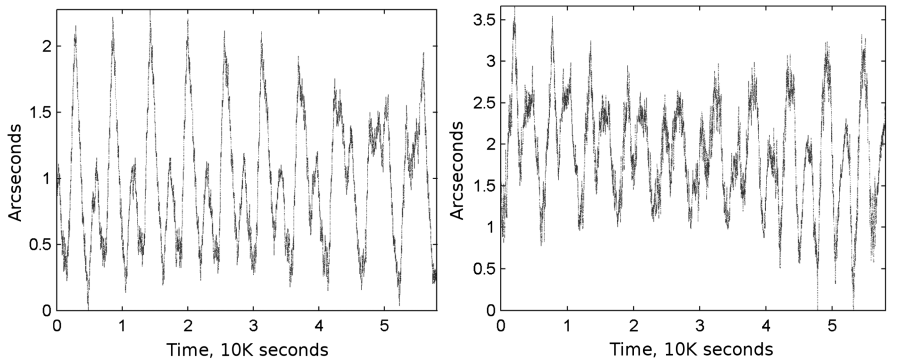

Fig. 10 Laser spot horizontal (left) and vertical (right) motion during orbits 16 through 25 of L2A.

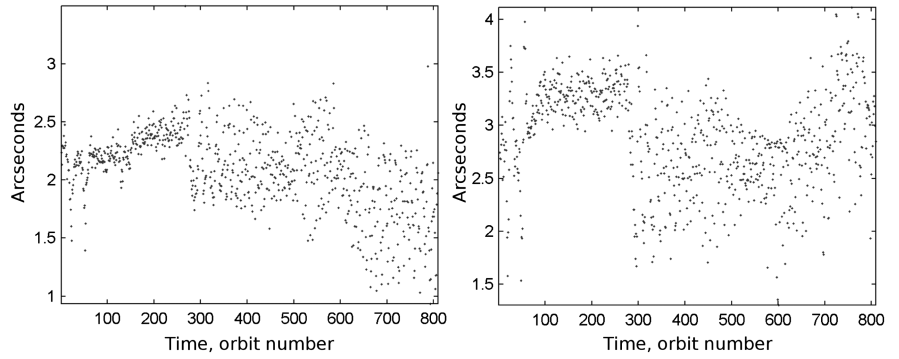

Fig. 11 Laser spot motion horizontal (left) and vertical (right) amplitudes during L2A.

standard deviations for Antarctica and Greenland with and without correction using the replacement method. These results do not include laser pointing bias corrections and saturation corrections that further reduce the uncertainties.

The L3C Greenland results are particularly interesting. During this campaign, the sun passes directly through the LRS and IST fields of view, blinding both instruments and producing increased relative motion between the LRS and IST. The uncorrected standard deviation of 61 cm is relatively large, and replacement method correction results in a relatively large reduction of uncertainty to 31 cm.

Figure 9 shows the laser spot motion in the LRS coordinate frame during orbits 16 through 25.

Time series of the laser spot horizontal and vertical motion during orbits 16 through 25 are shown in Fig. 10. During the first seven orbits, there are two peaks or oscillations of the laser motion per orbit in both the horizontal and vertical coordinates. The horizontal motion changes significantly in the last three orbits. The amplitudes of the peaks also vary significantly over these orbits. We believe that these variations and the structure of the points in Fig. 9 are evidence of changes in the laser beam, the retroreflectors redirecting the beam into the LRS, and relative motion between the LRS and laser transmitter.

The time series of horizontal and vertical amplitudes are shown in Fig. 11. The means and standard deviations are 2.1 ± 0.3 arcseconds for the horizontal amplitudes and 2.9 ± 0.5 arcseconds for the vertical amplitudes. As described earlier, there were two temperature events during L2A. Five outliers during the two temperature events were edited out of Fig. 11.

The overall objective for ICESat pointing knowledge is an uncertainty of 1.5 arcseconds 1σ or less, and the two to three arcsecond LRS to laser orbital variation is directly accounted for in the pointing processing. Compared to reference spot motion, laser spot motion and relative motion between the LRS and laser transmitter is relatively small. We believe that this is evidence that the relative motion between the LRS and the optical bench is also relatively small over orbital time scales.

VI. Conclusions

The explicit assumption behind the replacement method is that the relative motion between the Laser Reference Sensor (LRS), optical bench, and gyro unit is small and that pure-gyro propagation can track the attitude of the optical bench and LRS, given an adequate estimate of the gyro rate biases. The fact that the replacement method is able to reproduce significant features of the reference signal motion during L2A supports this assumption. Independent and more direct evidence is provided by the LRS laser spot observations. They support the inference that the relative motion between the LRS, optical bench, and laser system consists of orbital variations with amplitudes of 2 to 3 arcseconds.

Acknowledgements

The authors thank Scott Luthcke and John DiMarzio, both at NASA Goddard Space Flight Center, for their help, particularly with ocean scan and crossover analyses. This research was supported by NASA Grant NNX09AG20G.

References

[1] Bae, S., and Schutz, B. E., "Laser Pointing Determination Using Stellar Reference System in Geoscience Laser Altimeter System," *AAS/AIAA Space Flight Mechanics Meeting*, Vol. 105, Advances in the Astronautical Sciences, Paper AAS-00-123, Univelt, San Diego, CA, 2000, pp. 367–382.

[2] Schutz, B. E., Zwally, H. J., Shuman, C. A., Hancock, D., and DiMarzio, J. P., "Overview of the ICESat Mission," *Geophysical Research Letters*, Vol. 32, No. 21, 2005, pp. 1–4. doi:10.1029/2005GL024009

[3] Bae, S., Smith, N., and Schutz, B. E., "GLAS Precision Attitude Determination Algorithm Theoretical Basis Document 3.0," Center for Space Research, Austin, Report NASA TM-2012-208641, 2012.

[4] Bae, S., Schutz, B. E., and Sirota, J. M., "ICESAT/GLAS Laser Pointing Determination," *AAS/AIAA Spaceflight Mechanics Meeting*, Vol. 112, Advances in the Astronautical Sciences, Paper AAS-02-126, Univelt, San Diego, CA, 2002, pp. 359–370.

[5] Bae, S., and Schutz, B. E., "Star Tracker Relative Alignment Calibration and Its Application on Absolute Pointing Determination," *AAS/AIAA Astrodynamics Specialists Conference*, Vol. 109, Advances in the Astronautical Sciences, Paper AAS-01-312, Univelt, San Diego, CA, 2001, pp. 187–198.

[6] Bae, S., and Schutz, B. E., "System to Attain Accurate Pointing Knowledge of the Geoscience Laser Altimeter," *AAS Guidance and Control Conference*, Vol. 107, Advances in the Astronautical Sciences, Paper AAS-01-003, Univelt, San Diego, CA, 2001, pp. 39–48.

[7] Bae, S., Webb, C., and Schutz, B. E., "Star Tracker Misalignment Calibration for the ICESat Mission," *AAS/AIAA Space Flight Mechanics, Advances in the Astronautical Sciences*, Vol. 124, Advances in the Astronautical Sciences, Paper AAS-06-107, Univelt, San Diego, CA, 2006, pp. 113–124.

[8] Schutz, B. E., Bae, S., Smith, N., and Sirota, J. M., "Precision Orbit and Attitude Determination For ICESat," *F. Landis Markley Astronautics Symposium*, Vol. 132, Advances in the Astronautical Sciences, Paper AAS-08-305, Univelt, San Diego, CA, 2008, pp. 775–791.

[9] Brenner, A. C., DiMarzio, J. P., and Zwally, H. J., "Precision and Accuracy of Satellite Radar and Laser Altimeter Data Over the Continental Ice Sheets," *IEEE Transactions on Geoscience and Remote Sensing*, Vol. 45, No. 2, 2007, pp. 321–331. doi:10.1109/TGRS.2006.887172

[10] Luthcke, S. B., Rowlands, D. D., McCarthy, J. J., Pavlis, D. E., and Stoneking, E., "Spaceborne Laser-Altimeter-Pointing Bias Calibration from Range Residual Analysis," *Journal of Spacecraft and Rockets*, Vol. 37, No. 3, 2000, pp. 374–384. doi:10.2514/2.3571

[11] Luthcke, S. B., Carabajal, C. C., and Rowlands, D. D., "Enhanced Geolocation of Spaceborne Laser Altimeter Surface Returns: Parameter Calibration from the Simultaneous Reduction of Altimeter Range and Navigation Tracking Data," *Journal of Geodynamics*, Vol. 34, No. 3, 2002, pp. 447–475. doi:10.1016/S0264-3707(02)00047-9

[12] Bae, S., Smith, N., and Schutz, B. E., "ICESat Attitude and Pointing Correction Using the Laser Reference Sensor," *20th Spaceflight Mechanics Meeting*, Vol. 136, Advances in the Astronautical Sciences, Paper AAS-10-140, Univelt, San Diego, CA, 2010, pp. 621–635.

[13] Bae, S., and Schutz, B. E., "Precision Attitude Determination Using Gyro and Star Tracker Data with a Batch Least Squares Estimator," *AAS/AIAA Astrodynamics Conference*, Vol. 123, Advances in the Astronautical Sciences, Paper AAS-05-260, Univelt, San Diego, CA, 2005, pp. 175–182.

[14] Abshire, J. B., Sun, X., Riris, H., Sirota, J. M., McGarry, J. F., Palm, S., Yi, D., and Liiva, P., "Geoscience Laser Altimeter System (GLAS) on the ICESat Mission: On-orbit Measurement Performance," *Geophysical Research Letters*, Vol. 32, No. 21, 2005, pp. 1–4. doi:10.1029/2005GL024028

[15] Sirota, J. M., Bae, S., Millar, P., Mostofi, D., Webb, C., Schutz, B., and Luthcke, S., "The Transmitter Pointing Determination in the Geoscience Laser Altimeter System," *Geophysical Research Letters*, Vol. 32, No. 22, 2005, pp. 1–4. doi:10.1029/2005GL024005

[16] Markley, F. L., "Attitude Error Representation for Kalman Filtering," *Journal of Guidance, Control, and Dynamics*, Vol. 26, No. 2, 2003, pp. 311–317. doi:10.2514/2.5048

[17] Pittelkau, M. E., "Rotation Vector in Attitude Estimation," *Journal of Guidance, Control, and Dynamics*, Vol. 26, No. 6, 2003, pp. 855–860. doi:10.2514/2.6929

[18] Savage, P. G., "Strapdown Inertial Navigation Integration Algorithms Design Part 1: Attitude Algorithms," *Journal of Guidance, Control, and Dynamics*, Vol. 21, No. 1, 1998, pp. 19–28. doi:10.2514/2.4228

[19] Bayard, D. S., "High Precision Three-Axis Pointing and Control," *Encyclopedia of Aerospace Engineering: Attitude Dynamics and Orbit Control of Spacecraft*, edited by Blockley, R., and Shyy, W., Wiley, Hoboken, NJ, 2010, pp. 172–181.

[20] Markley, F. L., "Attitude Determination and Parameter Estimation Using Vector Observations: Application," *Journal of Astronautical Sciences*, Vol. 39, No. 3, 1991, pp. 367–381.

[21] Luthcke, S. B., Rowlands, D. D., Williams, T. A., and Sirota, J. M., "Reduction of ICESat Systematic Geolocation Errors and the Impact on Ice Sheet Elevation Change Detection," *Geophysical Research Letters*, Vol. 32, No. 21, 2005, pp. 1–4. doi:10.1029/2005GL023689

C. Kluever
Associate Editor